NANO MICRO small

Imaging

Three-Dimensional Exploration and Mechano-Biophysical Analysis of the Inner Structure of Living Cells

Álvaro Barroso, Mike Woerdemann, Angelika Vollmer, Gert von Bally, Björn Kemper, and Cornelia Denz**

***A** novel mechanobiological method is presented to explore qualitatively and quantitatively the inside of living biological cells in three dimensions, paving the way to sense intracellular changes during dynamic cellular processes. For this purpose, holographic optical tweezers, which allow the versatile manipulation of nanoscopic and microscopic particles by means of tailored light fields, are combined with self-interference digital holographic microscopy. This biophotonic holographic workstation enables non-contact, minimally invasive, flexible, high-precision optical manipulation and accurate 3D tracking of probe particles that are incorporated by phagocytosis in cells, while simultaneously quantitatively phase imaging the cell morphology. In a first model experiment, internalized polystyrene microspheres with 1 μm diameter are three-dimensionally moved and tracked in order to quantify distances within the intracellular volume with submicrometer accuracy. Results from investigations on cell swelling provoked by osmotic stimulation demonstrate the homogeneous stretching of the cytoskeleton network, and thus that the proposed method provides a new way for the quantitative 3D analysis of the dynamic intracellular morphology.*

1. Introduction

Intracellular and intercellular dynamics are essential for the development and maintenance of higher biological functions as well as are required in developing organisms, for both the formation of tissues and organs and their homeostasis.[1,2] Abnormal behavior of the cellular plasticity and mobility results in diseases, with common examples being cardiovascular and neurodegenerative diseases, inflammatory disorders, and especially tumor and metastasis in which respectively cells grow uncontrolled and migrate toward adjoining tissues and organs, respectively. The analysis of the biomechanics properties of cells is therefore of utmost scientific and medical interest.

The dynamics and rheological properties of the entire cell are determined at the molecular scale by the self-assembly and dynamics of the different subunits of proteins which form the filaments of the cytoskeleton, actin filaments, microtubules and intermediate filaments.[3,4] Thus, the analysis of the cell mechanics requires forces to be exerted on their inner structure and to investigate its response to this manipulation stimulus. In order to quantitatively analyse in a minimally-invasive way the micromechanical properties of living biological specimens at the single cell level, the manipulation method of choice has to ensure that the exerted external forces on the sample are non-destructive and in the biological relevant range of several tens of piconewton. Actual techniques are based on microfluidic manipulation, electromagnetic fields and optical forces interacting with the cell.[5–11]

Á. Barroso, Dr. M. Woerdemann, Prof. C. Denz
Institute of Applied Physics
University of Muenster
Corrensstrasse 2-4, 48149 Muenster, Germany
E-mail: denz@uni-muenster.de
A. Vollmer, Prof. G. von Bally, Dr. B. Kemper
Center for Biomedical Optics and Photonics
University of Muenster
Robert-Koch-Strasse 45, 48149 Muenster, Germany
E-mail: bkemper@uni-muenster.de

DOI: 10.1002/smll.201201851

Among these methods, laser light-based techniques are of particular importance since they provide contact-less manipulation of objects with a higher refractive index than the surrounding environment, as it is the case for cells and bacteria cultures. Single-beam gradient force optical traps, commonly named optical tweezers, are an established technique to manipulate organelles and internalized particles within adherent and suspended single cells.[12,13] Further on, holographic optical tweezers (HOT), which enable the generation and independent high-precise control of several 3D optical traps, have been demonstrated, for example, to rotate and translate multiple bacteria, to assemble three dimensional crystalline structures and to manage hierarchical supramolecular organization.[14] Furthermore, in combination with single-particle tracking methods, internalized particles can be utilized as micro- or nanoprobes to study inner cell properties. For instance, the track of the particle motion inside the cell, due to Brownian motion or caused by optical or magnetic induced forces, provides information about the viscosity of the cytoplasm, the diffusion parameters of particles within the cell, or the density and orientation of the polymer network of the cytoskeleton.[15–18]

Besides the use of particle tracking methods, the decipherment of the complex dynamics at the single cell level also requires novel techniques that provide additional information about dynamical changes of the cell morphology. In this respect, quantitative imaging prospects a tremendous boost in both development and application in basic and clinical cell research. Especially for the quantitative study of dynamic cellular processes, quantitative phase microscopy is more suitable than other qualitative imaging techniques such as bright field microscopy or differential interference contrast (DIC). Particularly, digital holographic microscopy (DHM) in off-axis configuration provides amplitude and quantitative phase information of the optical wave that propagates through a transparent sample.[19] This allows simultaneous quantitative phase imaging of the cell morphology as well as 3D tracking of transparent objects without fluorescence labeling.[19,20] Thus, the application and adaptation of multimodal strategies and the continuous development of novel quantitative imaging approaches that are minimally-invasive and marker free are therefore at the forefront of actual challenges.

Here, in order to investigate properties of the inner cell structure, we combine a HOT system with self-interference DHM.[21,22] The HOT system enables flexible 3D optical manipulation of the internalized particles within the cells while self-interference DHM provides simplified multi-focus quantitative phase imaging and 3D tracking. In contrast to previous promising works which combine DHM with conventional or holographic optical tweezers,[23–26] our approach provides the potential to explore the inner structure of living biological cells in three dimensions using optically manipulated particles as probes while simultaneous quantitative phase imaging of the cell morphology is provided. We first demonstrate the capability of this novel biophotonic approach to explore the inner structure of cells in three dimensions, and thus to sense tiny intracellular distances in the range of sub-micrometers between cellular compartments. Then, we exemplarily investigate dynamic changes of the internal cell structure that are produced by cell swelling due to osmotic stimulation. In combination with a characterization of the relevant parameters of living cells under isotonic and hypotonic conditions and an estimation of the optical forces that are applied to particles incorporated by living cells, we show that our approach provides a new way for 3D probing of the intracellular morphology without fluorescence labels.

2. Results and Discussion

2.1. Three-Dimensional Exploration of the Cell's Interior

First, we explore the internal structure of adherent cells by simultaneously manipulating internalized particles with HOT and mobility imaging with bright field microscopy and DHM, respectively. Pancreatic tumor cells (PaTu 8988T)[27] were selected as a model system and polystyrene (PS) spheres of 1 μm diameter as probes to explore the cell interior. These particles were chosen because of their non-toxicity[28,29] and the high refractive index ($n \approx 1.59$) of the material. Thus, the optical forces inside the cells were maximized and a high contrast in quantitative DHM phase images was produced. In addition, the diameter of the spheres was chosen in such a way that they could be resolved in quantitative DHM phase contrast and distinguished from intracellular organelles but also small enough to move the particles within the cellular scaffolding. The number of incorporated microspheres varied on each cell from any particle to more than ten. In the experiments, we focused the laser trapping beam on single particles which could not interact with other internalized particles during the experiment time. All investigations were performed on the HOT and DHM 'biophotonic workstation' depicted in **Scheme 1** at normal atmospheric conditions. In order to prevent overheating and fast cell migrations all experiments were performed at room temperature.[30] For details of this workstation and the sample preparation see the Experimental Section.

3D high-precision optical manipulation with HOT and particle tracking with DHM was performed with fixed position of the microscope objective. During the 3D manipulation of the particles within the cells with HOT digital holograms were recorded with an acquisition rate of 2 Hz. Then, amplitude and phase images were calculated from the reconstructed complex object wave and were analyzed to obtain the 3D particle trajectory and information of the cellular morphology.[20]

2.1.1. Axial Tracking of HOT Manipulated Particles within Cells by DHM

In contrast to other imaging techniques such as bright field microscopy or fluorescence microscopy, DHM allows to propagate numerically the reconstructed wave field of the sample from the hologram plane to the image plane where the sample appears in focus.[31] Since the movement of the internalized particles was carried out by HOT without moving the position of the microscope objective, the particles got out of focus when they were moved in the direction of the optical

DOI: 10.1002/smll.201201851

small NANO MICRO

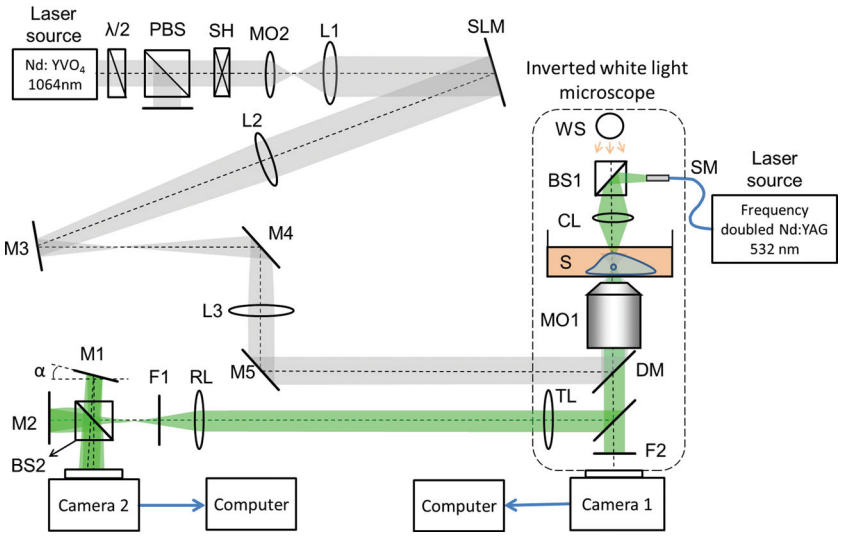

Scheme 1. Schematic of the combined DHM & HOT workstation used for 3D particle control and tracking of internalized spheres within cells. HOT elements: λ: rotatable half wave plate, PBS: polarizing beam splitter, SH: shutter, MO microscope objective, L:lens, SLM: spatial light modulator, M: mirror, DM: dichroic mirror, WS: white light source; DHM elements: SM: single mode optical fibre, BS: non-polarizing beam splitter, CL: condenser lens, TL: tube lens, RL relay lens, F: filter.

axis away from the observation plane. Subsequently, numerical refocusing was used together with a calibration of the optical imaging system (see supporting information) to track the axial movement of particles. In order to accelerate the numerical refocusing and axial tracking, holographic autofocusing was applied.[20]

Figure 1 illustrates dynamic axial digital holographic tracking of particles within a cell. Figures 1a,b show white light images of an adherent PaTu 8988T cell before and after moving one of the two internalized particles (particle A) with HOT. Due to the movement along the optical axis, particle A moved out of focus. Figures 1c,d show representative cross-sections (*x*-*z* plane) through focus stacks of DHM amplitude images that contain both particles. The amplitude images correspond to microscopic bright field images under coherent illumination and were generated by stacking 300 DHM amplitude images. The amplitude images were numerically reconstructed in different image planes from selected single off-axis holograms from a series of 38 digital off-axis holograms that were recorded during the particle movement with HOT. In this example, Particle B serves as static reference to check the axial displacement Δz of the optically manipulated particle A. To quantify the axial displacement, the distance required to propagate the reconstructed object wave to the image plane was determined. The axial displacements of particle A with respect to the initial trapping plane obtained from the whole hologram series is plotted in Figure 1e versus the axial position of the optical tweezers $z_{tweezers}$. The error for the axial particle localization is given by the accuracy of the numerical refocusing process. It depends on the individual light scattering properties of each cell and is determined in the ranges of 25 nm and 88 nm, respectively.

2.1.2. 3D Tracking of HOT-Manipulated Particles within Cells by Combined Axial and Lateral Tracking

The lateral movement of the particles was determined by the evaluation of the numerically focused quantitative phase images. Since the refractive index of the employed

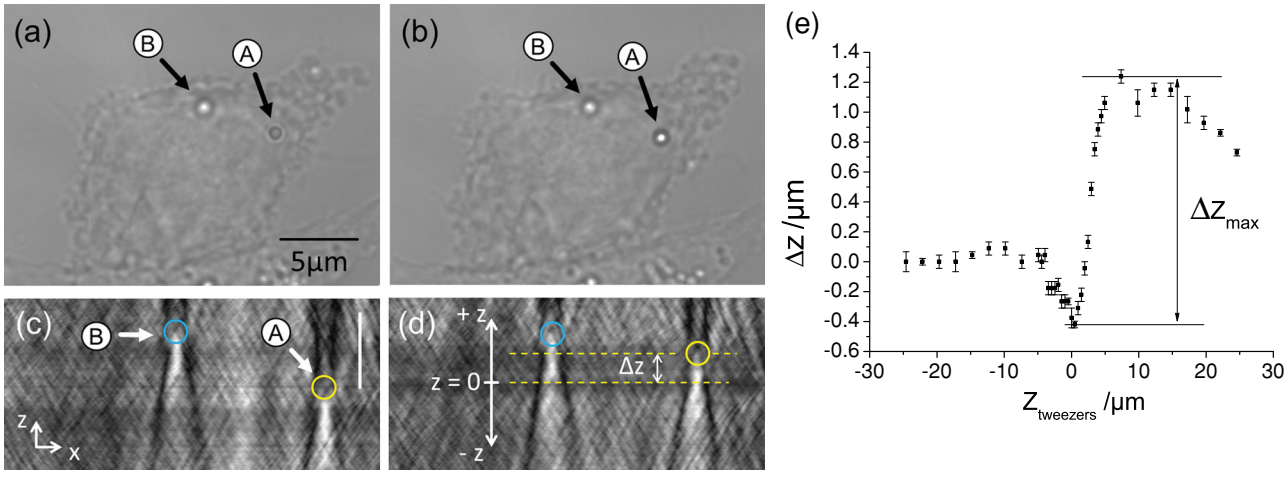

Figure 1. (a,b) White light images of an adherent PaTu 8988T cell with two incorporated 1 µm polystyrene particles before and after optical manipulation of particle A in the axial direction while particle B is used as reference. (c,d) Corresponding cross section images in the *x*-*z* plane containing both particles obtained from a stack of 300 DHM amplitude images that were reconstructed by numerical refocusing from a single digital hologram. The distance Δz required to propagate the image from the plane where the particle is initially in focus (z = 0) to the image plane is used to quantify the movement of the particle in axial direction. Scale bar 5 µm. (e) Axial position of particle A versus the axial focus position $z_{tweezers}$ of the optical trap.

DOI: 10.1002/smll.201201851

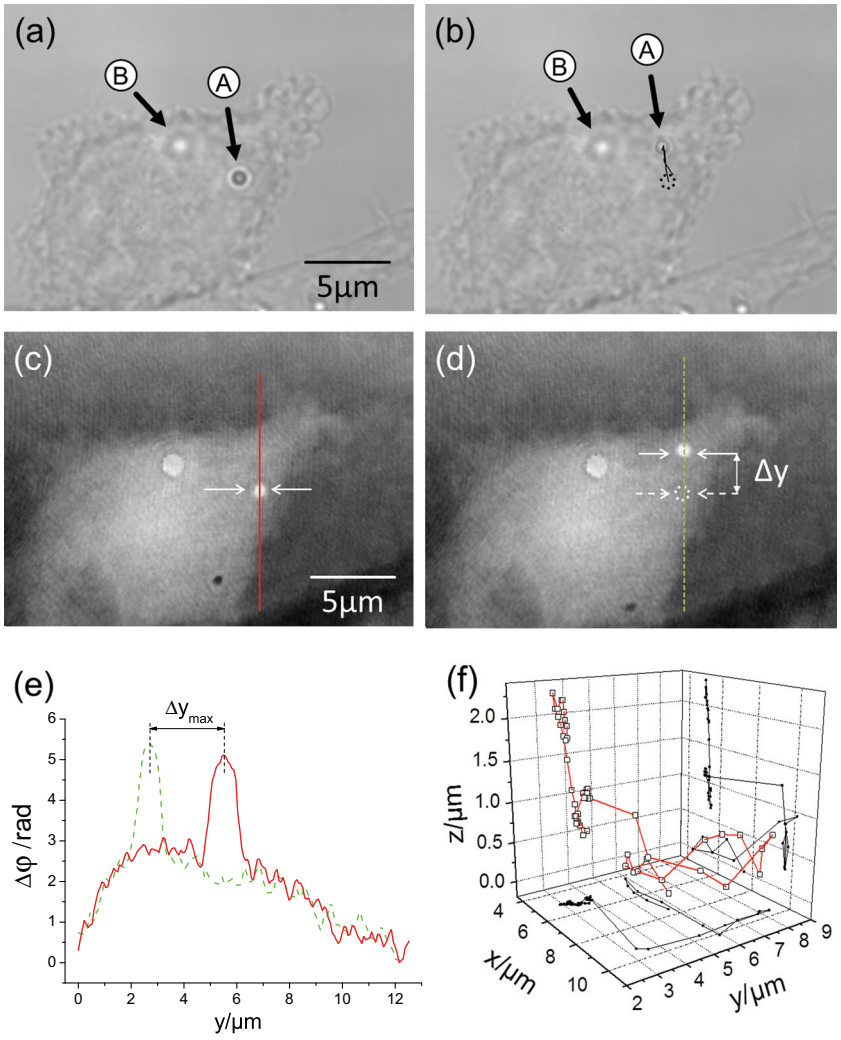

Figure 2. (a,b) White light images and (c,d) DHM phase images of the same PaTu 8988T cell in Figure 1. Particle A is moved in the lateral *y*-direction. (e) Cross sections along the continuous red line and dashed green line, respectively, through the phase images in (c) and (d). The dynamic lateral tracking of the particle that is obtained from the spatial coordinates of the point with maximum phase contrast in the phase images is illustrated in (b). (f) 3D trajectory of the particle obtained by combining the lateral and axial trajectories.

microspheres was larger than the refractive index of the cellular specimens, a high local maximum $\Delta\phi_{max}$ in the quantitative phase images was produced at the position of the particles. Thus, after calibrating the image scale the pixel coordinates of the point with maximum phase contrast determine the lateral spatial coordinates of the sphere.[20] In order to obtain the full 3D trajectory of the particles the procedure for two-dimensional particle tracking was combined with axial tracking.

Figure 2 illustrates the lateral tracking by DHM of a polystyrene sphere that was moved by HOT in *y*-direction within an adherent PaTu 8988T cell. The large difference between the refractive index of the PS particle and the refractive index of the cytoplasm produced a phase retardation of nearly 2.5 rad which results in a high phase contrast at the position of the particle. Figure 2e illustrates the phase profile $\Delta\phi$ along the direction of movement at different positions of the particle during the lateral movement. The distance Δy between the two local maxima of the phase distribution was determined with pixel accuracy to quantify the lateral displacement between successive movement steps. The particle could be moved only within a limited region of the cytoplasm due to cellular constraints like the plasma membrane, the nucleus or areas with a high density of cytoskeleton filaments. In addition, the cross sections through the phase contrast images show no morphology changes of the cell during the experiment time (~3 min). This indicates that no significant photodamage was induced by the optical tweezers beam.[30] The uncertainty of the lateral particle tracking was determined to be 80 nm and it was calculated from the position fluctuation that was measured from the phase images of 100 independent digital holograms that were captured of an optically trapped suspended particle. Figure 2f shows the complete 3D trajectory of the particle movement that was obtained after evaluation of the sharply focused DHM phase contrast images of the particle.

Probing the inside of a cell with a particle as show in Figure 2 provides useful information about the intracellular structure. Thus, the mobility of the particles within the cells was systematically characterized by measuring the maximum distances Δx_{max}, Δy_{max} and Δz_{max} that the particles were displaced in each direction. **Figure 3** shows the optically-induced maximum displacement of 20 internalized polystyrene particles in comparison to the Brownian motion that was detected without using HOT. It becomes visible that the available intracellular space to move the particle depends on each individual cell. However, in all cases higher lateral displacements were measured when the particle was moved with optical tweezers. Also for axial manipulation with HOT, higher displacements were achieved in most cases. In two cases we measured an abnormally large displacement of the internalized particles in the axial direction without the use of the optical tweezers. We suspect that this was caused by intracellular transport through the cytoskeleton network. In Figure 3d, the average maximum displacements $\overline{\Delta x}_{max}$, $\overline{\Delta y}_{max}$ and $\overline{\Delta z}_{max}$ are shown. The error bars are given by the standard deviation from the mean value. The average maximum displacement demonstrates the capability of the trapping beam to move the particle within the cell volume. The asymmetry that is found between the particle mobility in lateral and axial direction may be explained by the morphology of the adherent cells which have a typical diameter in the range of ~20 µm that is larger than the cell thickness of about ~10 µm (see Section 2.2).[31] In addition, another parameter to consider in the

small 2012,
DOI: 10.1002/smll.201201851

NANO MICRO small

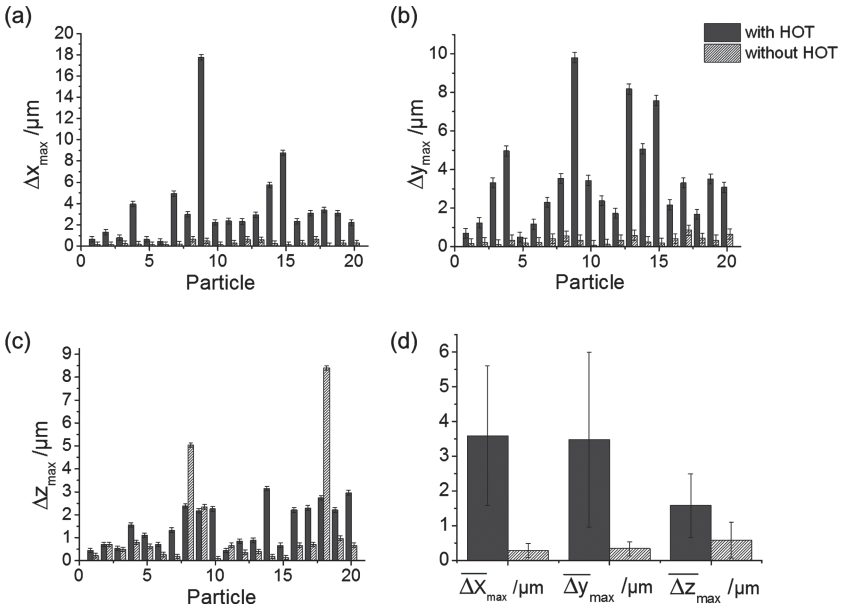

Figure 3. (a–c) Maximum displacements in the three directions Δx_{max}, Δy_{max} and Δz_{max} that were measured with DHM from the motion of 20 polystyrene particles (1 µm of diameter) that were incorporated in different adherent PaTu 8988T cells. (d) Average maximum displacements obtained from the data in (a–c). Dark and light bars indicate the particle displacements that were measured using HOT and without any treatment, respectively.

interpretation of the results in Figure 3 is the quality of the optical trap, which changes during the steering in the direction of the optical axis. A calibration of the optical trap in this direction (see Supporting Information) shows that spherical aberrations in the trapping beam are typically observed from 3 µm above the focal plane of the microscope objective. This indicates a decrease of the depth of the potential well along the steering in z-direction and thereby a lower strength of the optical trap.[32]

2.2. Investigation of Intracellular Changes During Osmotic Stimulation

Having demonstrated the capability of the proposed method to quantify distances within intracellular compartments, we evaluated in a next step the sensing of cell morphology changes during cell swelling that is provoked by osmotic stimulation. For this purpose, the adherent cells with PS internalized particles were investigated in isotonic cell culture medium (DMEM buffered with Hepes) with an osmolality determined with an osmometer of 320 mOsmol kg^{-1} and in an hypotonic medium (160 mOsmol kg^{-1}) that was obtained by dilution of the initial medium with deionized water.

2.2.1. Cell Swelling Characterization

In preliminary investigations, we analyzed cell thickness changes due to osmotically induced water influx with quantitative DHM phase contrast. For cells in cell culture medium with refractive index n_{medium}, and assuming a known homogeneously distributed integral cellular refractive index cell n_{cell}, the cell induced optical phase retardation $\Delta\phi_{cell}$ to the extracellular medium dependents on the cell thickness d_{cell}:[19]

$$\Delta\varphi_{cell}(x, y) = \frac{2\pi}{\lambda}(n_{cell} - n_{medium})\, d_{cell}(x, y), \quad (1)$$

where λ is the light wavelength used for DHM. Thus, information about the cellular refractive index is essential to obtain reliable values for the cells thickness. For this purpose, the parameter n_{cell} was obtained with the assumption to be equal to the refractive index of the cytoplasm $n_{cytoplasm}$ with a DHM-based method. In this case the same PS particles that were utilized in this study to explore the intracellular space could be also used inside the cells as a reference with a known refractive index.[33] Thus, the refractive index of the cytoplasm was directly calculated from quantitative DHM phase images.

Table 1 shows the obtained averaged refractive index of the cytoplasm $\bar{n}_{cytoplasm}$ that was measured with 15 particles incorporated in 15 different cells under isotonic and hypotonic conditions. The values were validated by comparative determination of the integral cellular refractive index $\bar{n}_{cell}$ of suspended cells with spherical shape (see Supporting Information).[34] As expected from the water influx due to the osmosis, the refractive index decreased from isotonic to hypotonic conditions. Within the statistical uncertainty for both, suspended and adherent cells, similar refractive index values were obtained. Therefore, it is sufficient to assume a homogeneous cellular refractive index in order to analyze the cell thickness during the cell swelling. Considering the refractive index values in Table 1 and the refractive indices of the extracellular medium ($n_{DMEM,\,320}$ = 1.339 ± 0.001 and $n_{DMEM,\,160}$ = 1.337 ± 0.001, determined with an Abbe refractometer) the cell thickness can be straightforwardly determined from quantitative DHM phase images using Equation 1. **Figure 4** shows the swelling of a representative adherent cell from isotonic to hypotonic conditions. The cell thickness increases nearly by a factor two after changing the osmolality from 320 mOsmol kg^{-1} to 160 mOsmol kg^{-1}. This correlates with data from comparative DHM investigations on adherent and suspended cells in which near doubling of the cell volume was observed.[35,36]

The refractive index difference between an internalized particle and the surrounding cytoplasm determines the stiff-

Table 1. Mean cytoplasm refractive index $\bar{n}_{cytoplasm}$ and mean integral cellular refractive index $\bar{n}_{cell}$ of suspended PaTu 8988T cells for different osmolality of the cell culture medium. $N_{adherent}$, $N_{suspended}$: Number of measurements.

Medium	Osmolality [mOsmol kg^{-1}]	$\bar{n}_{cytoplasm}$	$N_{adherent}$	$\bar{n}_{cell}$	$N_{suspended}$
Hypotonic	160 ± 1	1.356 ± 0.013	15	1.358 ± 0.003	57
Isotonic	320 ± 1	1.372 ± 0.012	15	1.365 ± 0.003	57

DOI: 10.1002/smll.201201851

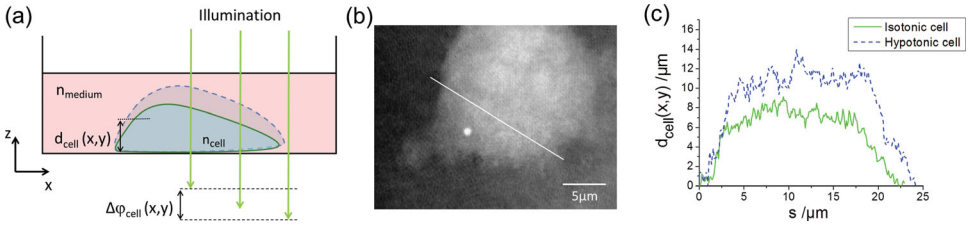

Figure 4. DHM analysis of osmotically induced cell swelling. (a) The phase retardation $\Delta\phi_{cell}$ of the light that passes through a cell is caused by the cell thickness $d_{cell}(x,y)$ and the refractive index difference between the cell and the surrounding medium $\Delta n = n_{cell} - n_{medium}$. The cell swells due to osmosis when the osmolality of extracellular medium is decreased by addition of deionized water. (b) DHM phase image of an adherent PaTu 8988T cell with an incorporated 1 µm polystyrene particle. (c) Cell thickness $d_{cell}(x,y)$ calculated from the cross-section through the quantitative DHM phase image in (b) under isotonic (green continuous line) and hypotonic (blue dashed line) conditions.

ness of the optical trap and the maximal optical force that can be applied to move the particles.[37] Thus, we estimated the maximal force F_{trap} of the optical trap that was applied to move the particles within the PaTu 8988T cells under hypotonic and hypertonic conditions by experimental simulation of the intracellular environment using the drag force method (see supporting information). The resulting maximum optical trapping force for the power used in the experiments described in Sections 2.1.2 and 2.2.2, P = 180 mW at the back side of the inverted microscope, amounted for isotonic cells to (31.8 ± 1.1) pN while for hypotonic cells a force of (31.9 ± 0.9) pN was obtained. This indicates that within the measurement uncertainty, the optical forces exerted on particles were equal within the used PaTu 8988T cells under isotonic and hypotonic conditions.

2.2.2. Sensing Dynamic Changes in the Cytoskeleton

In order to investigate whether the method described in Section 2.1 is capable to detect inner changes of the cell structure, the mobility of 20 engulfed 1 µm PS spheres in 20 different PaTu 8988T cells was analyzed for isotonic and hypotonic conditions. In each measurement, a microsphere was first moved with HOT in three dimensions in isotonic cells while digital holograms were captured with an acquisition rate of 2 Hz. Then, the measurement procedure was repeated in the same cells under hypotonic conditions after the dilution of the extracellular medium to 160 mOsmol kg^{-1}.

Figures 5a–c show the maximum intracellular displacements Δx_{max}, Δy_{max} and Δz_{max} of the particles in 20 different cells for isotonic and hypotonic conditions. Figures 5d–f depict the corresponding averaged maximum displacements. For all three spatial directions an increase of the particle mobility is observed from isotonic to hypotonic cells. Moreover, similar differences δx = 1.3 µm, δy = 1.0 µm and δz = 1.0 µm are obtained in the particle mobility between isotonic and hypotonic conditions. It has been reported that diffusion of particles within a cell not only depends on its size but also on the density of proteins in the areas where the particles are engulfed.[15] Thus it is expected that the optical-tweezers-induced movement of particles was influenced by the cytoskeleton network. Since the optical forces that were applied to move the particles were the same in normal and swollen cells, the isotropic increase of the particle mobility may be explained by homogeneous stretching of the cytoskeleton network during the cell swelling process.

2.3. Influence of the Tubulin Density on the Particle Movement

In order to check if the particle mobility is indeed related to the density of the cytoskeleton filaments, we performed a comparative investigation with fluorescence microcopy to localize the position of the particles within the tubulin filaments. For this purpose, in living PaTu 8988T cells tubulin was labeled with Green Fluorescence Protein (GFP) and the manipulation of the internalized polystyrene particles was observed with both bright field microscopy under white light illumination and fluorescence microscopy. In order to avoid photobleaching under long term observation, fluorescence images were taken after the optical manipulation of the particles.

Figure 6 shows representative white light and fluorescence images of two different adherent PaTu 8988T cells with incorporated particles. The white light images illustrate the initial and final position of the particle after the manipulation with the optical trap. The fluorescence images show the tubulin distribution inside the cell. After calibration of the image scale, the lateral displacement can be roughly estimated in each case. It is observed that in Figures 6a,b the particle stays almost at the same position, with a displacement of less than 1 µm (the particle remains inside the circle) during the manipulation with HOT. In Figures 6d,e, it is observed that the particle can be moved for a larger distance of about 3.5 µm (the particle is even out of the circle). The comparison of the fluorescence images with the HOT-induced particle movements shows that the small displacement of the first particle correlates with a high tubulin density while the higher movability of the second particle is observed in an area with a low density of tubulin. This first result indicates in a plausible way that the particle mobility is directly related to the density of the microtubule network.

3. Conclusion

In this proof-of-principle study, we have demonstrated that holographic optical tweezers combined with self-interference digital holographic microscopy are an ideal multimodal workstation for quantifying changes of the intracellular space of living cells by using polystyrene microspheres as non-toxic microprobes. In comparison with previously

small 2012,
DOI: 10.1002/smll.201201851

small NANO MICRO

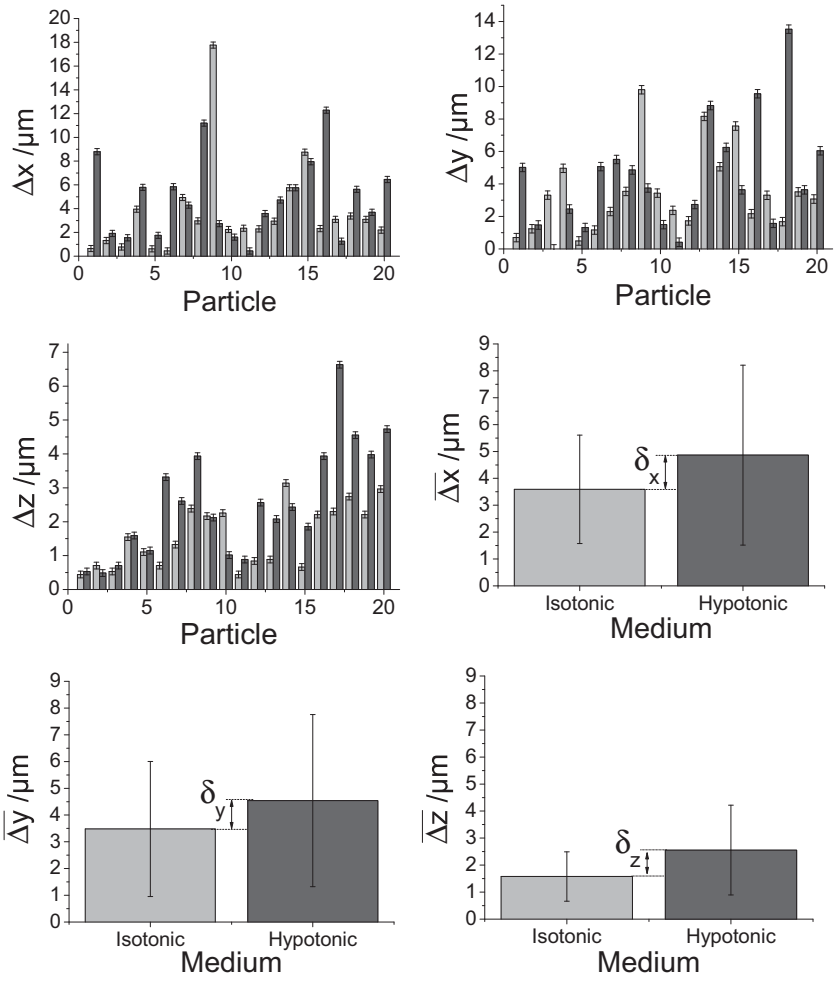

Figure 5. (a–c) Maximum displacements in *x*, *y* and *z* direction of 20 internalized particles that were moved within 20 different adherent PaTu 8988T cells under isotonic (pale bars) and hypotonic conditions (dark bars). (d–f) Average maximum displacements for the movement of the 20 different particles of (a–c).

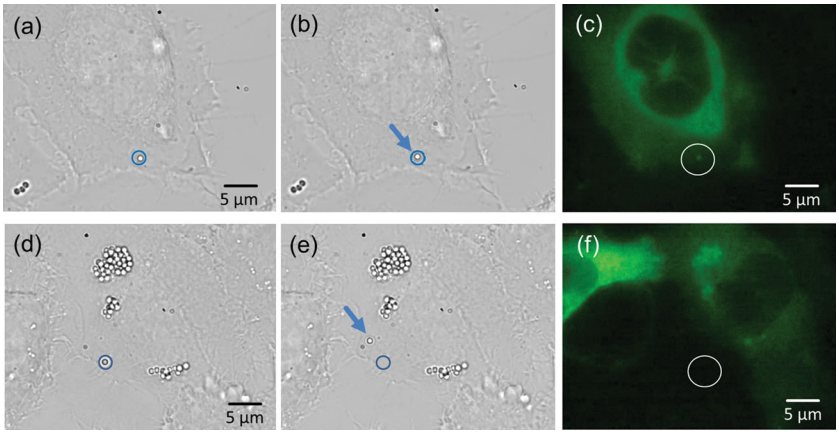

Figure 6. Localization of particles within the cytoskeleton by fluorescence microscopy. (a,d) White light images of PaTu 8988T cells with internalized 1 µm PS particles before using the optical tweezers to move the particles and corresponding (b,e) white light images and (c,f) fluorescence images after manipulation of the particles. Tubulin was stained with GFP. The circles mark the initial position of the particles inside the cytoskeleton. The arrows indicate the position of the bead after the movement with HOT.

reported particle tracking methods, our concept has the potential of providing quantitative mechano-biophysical information of the cell interior in three dimensions without fluorescence labeling while simultaneously information about the cell morphology is provided. In addition, within the observation time, no changes of the cell morphology in the quantitative DHM phase contrast are observed. This demonstrates that our method is minimally invasive as neither the trapping laser beam nor the imaging laser source induces serious damage to the investigated cells.

The results from the cell interior exploration further show that our approach allows performing highly precise 3D manipulation and localization of sensor particles within living cells with submicrometer accuracy. In comparison to the Brownian motion of the internalized particles in the cytoplasm, we showed that significant higher defined displacements of the particles are achieved using optical tweezers. The optically induced movement was limited by the cell boundaries and thereby provided direct information about the inner cell structure.

The DHM metrology feature of the utilized biophotonic workstation was also used in combination with optical manipulation and tracking of the probing particles to study the swelling process of living cells from isotonic to hypotonic conditions. Changes of the intracellular refractive index and the cell thickness could be analyzed in the same cells and with the same polystyrene particles that were later used as probes to explore the intracellular space. Furthermore, the precise determination of the cellular refractive indices cells reveals that DHM delivers essential data to estimate the optical forces that are applied to the particles within the cytoplasm. The magnitudes of the forces which were obtained experimentally in the range of tens of piconewtons are in agreement to data that have been previously determined in the manipulation of biological specimens by using a fibre optical two beam trap or magnetic tweezers.[5,38] Finally, probing of the intracellular space during osmotic stimulation demonstrated the feasibility of our approach to quantify changes in the structure of the cytoskeleton. Since the optical forces remain constant for normal and swollen cells, the increase of the available intracellular

DOI: 10.1002/smll.201201851

space to move the particle can be explained by the stretching of the cytoskeleton filaments during the cell swelling.

In conclusion, we have shown that the combined implementation of holographic optical tweezers, digital holographic microscopy, and microspheres as sensitive probes inside cells provides a novel mechanobiological tool for minimally-invasive quantitative 3D probing of the intracellular morphology without any fluorescence labels. We further believe that the technique has a high potential to become a new tool in cell microrheology and cellular biomechanics, as e.g. for measuring the diffusivity of particles within living cells.

4. Experimental Section

Sample Preparation and Experimental Conditions: Human pancreatic tumor cells (PaTu 8988T)[27] were cultured at 37 °C in 10% CO2 atmosphere in Dulbecco's modified Eagle's medium (DMEM) with 3.7 g/L NaHCO3, 580 mg/L L-glutamine, 110 mg/L Na-pyruvate, 4.5 g/L D-glucose (DMEM FG0455 Biochrom, Berlin, Germany) and supplemented with 5% fetal calf serum (FCS of PAA, Pasching, Austria) and 5% horse serum (HS of Biochrom, Berlin, Germany). The cells were incubated for one night with polystyrene (PS) microspheres in Petri dishes with a physical treated bottom (μ-Dish ibiTreat, ibidi GmbH, Munich, Germany). Prior to the experimental investigations with HOT and DHM, the cells were washed twice with DMEM to remove non-incorporated microspheres and to avoid disturbances in the DHM phase contrast or trapping of undesirable particles by the optical tweezers. Straight afterwards, the cell medium was replaced by DMEM buffered with Hepes to prevent intracellular acidosis at normal atmosphere. In order to change the internal cell morphology, cells were osmotically swollen by dilution of the isotonic cell culture medium (320 mOsmol kg^{-1}) to a final hypotonic medium (160 mOsmol kg^{-1}). For imaging with fluorescence microscopy, adherent cells were labeled with a green fluorescence protein GFP (CellLight® Tubulin-GFP, BacMam 2.0 C10613, Life Technologies GmbH Invitrogen, Darmstadt, Germany).

Experimental Setup: For simultaneous manipulation and tracking of the particles in three dimensions a holographic optical tweezers system (HOT) and a modular self-interference digital holographic microscopy setup (DHM) were implemented on a commercial inverted fluorescence microscope (Eclipse Ti, Nikon) with a high numerical aperture microscope objective (MO1) (Nikon Apo TIRF, 100x/1.49 Oil-immersion). Scheme 1 shows a schematic of the workstation. For optical trapping a Neodymium-doped Yttrium Orthovanadate (Nd:YVO_4) laser operating at a wavelength λ = 1064 nm and a maximum output power P = 2.5 W is utilized. A phase-only spatial light modulator (SLM) (Holoeye, Pluto, 1920 × 1080 pixels, Holoeye Berlin, Germany) and a custom-made software[39] are used to modulate the light beam of the laser in order to control and steer three-dimensionally the optical trap.[21] Camera 1 (Pixely qe, PCO, Kelheim, Germany) is used together with the software to control the focus of the trapping beam. In order to have a compromise between sufficiently high forces and low photodamage on the biological specimen the power was set to 180 mW at the back side of the inverted microscope.[30] The manipulation of the incorporated PS particles is observed by bright field imaging and quantitative DHM phase contrast. For this purpose, the coherent light of a frequency-doubled neodymium-doped yttrium aluminum garnet (Nd:YAG) laser (λ = 532 nm) is introduced into the white light illumination path of the inverted microscope using a single mode (SM) optical fibre and a non-polarizing beam splitter (BS1). The microscope condenser lens (CL) is adjusted to provide suitable illumination similar to Koehler illumination.[31] The microscope objective MO1, a tube lens (TL) and a relay lens (RL) are used to magnify the sample (S). Then, the object wave enters in a Michelson interferometer formed by two mirrors (M1 and M2) and a second beam splitter (BS2). In order to produce a suitable spatial carrier interference fringe pattern for off-axis holography, one mirror M1 is tilted by a small angle α in such a way that an area of the sample that contains no object is superposed with the image of the specimen.[22] The resulting interference pattern (digital hologram) is recorded by a charge coupled device sensor (Camera 2) (CCD, The Imaging Source DMK 41BU02, Bremen, Germany) and transferred to a computer for numerical reconstruction by spatial phase shifting.[31,40] If the object has been recorded out-of-focus, optionally autofocusing of the sample is provided by DHM.

Supporting Information

Supporting Information is available from the Wiley Online Library or from the author.

Acknowledgements

This work was supported by the Deutsche Forschungsgemeinschaft in the frame of the German-Chinese TRR61. Further financial support by the German Ministry of Education and Research (BMBF) within the research focus program "Biophotonics" (FKZ13N10937) and the Cluster of Excellence "Cells in Motion" (EXC 1003/1), the European Union funded Erasmus Program and the University of Sevilla are gratefully acknowledged. The authors would like to thank Christina Alpmann, Lena Dewenter and Florian Hörner from the Nonlinear Photonics Group, Institute of Applied Physics, for helpful discussions.

[1] E. Papusheva, C.-P. Heisenberg, *EMBO J.* **2010**, *29*, 2753.
[2] G. A. Gomez, R. W. McLachlan, A. S. Yap, *Trends Cell Biol.* **2011**, *21*, 499.
[3] B. Alberts, A. Johnson, J. Lewis, M. Raff, K. Roberts, P. Walter, in *Molecular Biology of the Cell*, Vol. *1* (Eds: B. Alberts, J. Wilson, T. Hunt), Garland Science, New York **2002**, Ch.16.
[4] P. A. Janmey, *Curr. Opin. Cell Biol.* **1991**, *3*, 4.
[5] J. Guck, R. Ananthakrishnan, H. Mahmood, T. J. Moon, C. C. Cunningham, J. Käs, *Biophys. J.* **2001**, *81*, 767.
[6] J. Voldman, *Annu. Rev. Biomed. Eng.* **2006**, *8*, 425.
[7] A. H. B. de Vries, B. E. Krenn, R. van Driel, J. S. Kanger, *Biophys. J.* **2005**, *88*, 2137.
[8] W. Feneberg, M. Westphal, E. Sackmann, *Eur. Biophys. J.* **2001**, *30*, 284.
[9] M. Manimaran, E. H. T. Francis, K. C. Chaw, *J. Phys. Conf. Ser.* **2006**, *34*, 1143.

DOI: 10.1002/smll.201201851

[10] D. J. Stevenson, F. Gunn-Moore, K. Dholakia, *J. Biomed. Opt.* **2010**, *15*, 041503.
[11] K. Svoboda, S. M. Block, *Annu. Rev. Biophys. Biomol. Struct.* **1994**, *23*, 247.
[12] A. Ashkin, J. M. Dziedzic, T. Yamane, *Nature* **1987**, *330*, 769.
[13] I. A. Vorobjev, H. Liang, W. H. Wright, M. W. Berns, *Biophys. J.* **1993**, *64*, 533.
[14] M. Woerdemann, C. Alpmann, C. Denz, in *Optical Imaging and Metrology* (Eds: W. Osten, N. Reingand), Wiley-VCH Verlag, Weinheim, Germany, **2012**, pp.179–206.
[15] A. Caspi, R. Granek, M. Elbaum, *Phys. Rev. E.* **2002**, *66*, 011916.
[16] D. Wirtz, *Annu. Rev. Biophys.* **2009**, *38*, 301.
[17] T. Kalwarczyk, N. Ziebacz, A. Bielejewska, E. Zaboklicka, K. Koynov, J. Szymański, A. Wilk, A. Patkowski, J. Gapiński, H.-J. r. Butt, R. Hołyst, *Nano Lett.* **2011**, *11*, 2157.
[18] V. M. Laurent, S. Henon, E. Planus, R. Fodil, M. Balland, D. Isabey, F. Gallet, *J. Biomech. Eng.* **2002**, *124*, 408.
[19] B. Kemper, G. von Bally, *Appl. Opt.* **2008**, *47*, A52.
[20] P. Langehanenberg, L. Ivanova, I. Bernhardt, S. Ketelhut, A. Vollmer, D. Dirksen, G. Georgiev, G. v. Bally, B. Kemper, *J. Biomed. Opt.* **2009**, *14*, 014018.
[21] M. Woerdemann, S. Glasener, F. Horner, A. Devaux, L. De Cola, C. Denz, *Adv. Mater.* **2010**, *22*, 4176.
[22] B. Kemper, A. Vollmer, C. E. Rommel, J. Schnekenburger, G. von Bally, *J. Biomed. Opt.* **2011**, *16*, 026014.
[23] S.-H. Lee, D. G. Grier, *Opt. Express* **2007**, *15*, 1505.
[24] N. Cardenas, L. Yu, S. K. Mohanty, *Proc. of SPIE* **2011**, *7902*, 79020U.
[25] M. Esseling, B. Kemper, M. Antkowiak, D. J. Stevenson, L. Chaudet, M. A. A. Neil, P. W. French, G. von Bally, K. Dholakia, C. Denz, *J. Biophotonics* **2012**, *5*, 9.
[26] M. DaneshPanah, S. Zwick, F. Schaal, M. Warber, B. Javidi, W. Osten, *J. Disp. Technol.* **2010**, *6*, 490.
[27] H.-P. Elsässer, U. Lehr, B. Agricola, H. Kern, *Virchows Archiv. B Cell Pathol.* **1992**, *61*, 295.
[28] P. A. Revell, *Nanotechnol. Perceptions: Rev. Ultraprecision Engin.* **2006**, *2*, 283.
[29] U. O. Häfeli, G. J. Pauer, *J. Magn. Magn. Mater.* **1999**, *194*, 76.
[30] Á. Barroso, B. Kemper, M. Woerdemann, A. Vollmer, S. Ketelhut, G. v. Bally, C. Denz, *Proc. of SPIE* **2012**, *8427*, 842701A1.
[31] B. Kemper, D. Carl, J. Schnekenburger, I. Bredebusch, M. Schafer, W. Domschke, G. von Bally, *J. Biomed. Opt.* **2006**, *11*, 34005.
[32] E. Florin, A. Pralle, E. S. J. Horber, *Appl. Phys. A* **1998**, *66*, S75.
[33] B. Kemper, S. Przibilla, A. Vollmer, S. Ketelhut, G. von Bally, *Proc. of SPIE* **2011**, *8086*, 808607.
[34] B. Kemper, S. Kosmeier, P. Langehanenberg, G. von Bally, I. Bredebusch, W. Domschke, J. Schnekenburger, *J. Biomed. Opt.* **2007**, *12*, 054009.
[35] B. Rappaz, P. Marquet, E. Cuche, Y. Emery, C. Depeursinge, P. Magistretti, *Opt. Express* **2005**, *13*, 9361.
[36] B. Kemper, J. Klokkers, S. Przibilla, A. Vollmer, S. Ketelhut, G. von Bally, E. Schlatter, H. Pavenstädt, B. Edemir, *Phot. Lett. of Poland* **2012**, *4*, 45.
[37] K. C. Neuman, S. M. Block, *Rev. Sci. Instrum.* **2004**, *75*, 2787.
[38] A. H. B. de Vries, B. E. Krenn, R. van Driel, V. Subramaniam, J. S. Kanger, *Nano Lett.* **2007**, *7*, 1424.
[39] D. Preece, R. Bowman, A. Linnenberger, G. Gibson, S. Serati, M. Padgett, *Opt. Express* **2009**, *17*, 22718.
[40] D. Carl, B. Kemper, G. Wernicke, G. von Bally, *Appl. Opt.* **2004**, *43*, 6536.
[41] P. Langehanenberg, G. v. Bally, B. Kemper, *3D Res.* **2011**, *2*, 1.
[42] S. Kosmeier, B. Kemper, P. Langehanenberg, I. Bredebusch, J. Schnekenburger, A. Bauwens, G. von Bally, *Proc. of SPIE* **2008**, *9*, 1.
[43] J. Vörös, *Biophys. J.* **2004**, *87*, 553.

Received: July 31, 2012
Published online: